Journal of Magnetic Resonance **149,** 110–113 (2001)
doi:10.1006/jmre.2000.2278, available online at http://www.idealibrary.com on IDEAL®

# COMMUNICATIONS

## Simultaneous Determination of Orientational and Order Parameter Distributions from NMR Spectra of Partially Oriented Model Membranes

Edward Sternin,* Hartmut Schäfer,† Ivan V. Polozov,‡ and Klaus Gawrisch‡

*Department of Physics, Brock University, St. Catharines, Ontario L2S 3A1, Canada; †HF-NMR Facility, University of Nijmegen, 6525 ED Nijmegen, The Netherlands; and ‡Laboratory of Membrane Biochemistry and Biophysics, NIAAA, NIH, 12420 Parklawn Drive, Rockville, Maryland 20852
E-mail: edik@brocku.ca; hasc@solidmr.kun.nl; polozov@sammy.niaaa.nih.gov; gawrisch@helix.nih.gov

Received May 22, 2000; revised December 11, 2000

There are significant advantages to orienting complex molecules if one is attempting to determine their structure or characterize intramolecular motions. One typically explores chemical shift, dipolar, or quadrupolar interactions to reveal the pattern of bonds or geometrical constraints that determine the spatial relationships between constituent atoms. The strength of such interactions usually depends on the orientation relative to the external magnetic field. In the case of an axially symmetric second-rank tensorial interaction, this dependence typically involves $P_2(\cos\theta) = \frac{1}{2}(3\cos^2\theta - 1)$ with the angle $\theta$ between the magnetic field and the symmetry axis of the interaction. This scales the interaction by a factor between 1 and $-0.5$ (including zero at the "magic angle"), and the resulting spectra are broad powder averages, or superpositions of contributions from all possible orientations present in the sample.

To restore the resolution, one needs to somehow separate the orientational distribution of all the angles that a given interaction (typically, molecular) axis may have with respect to the magnetic field from a set of anisotropies that define the interaction strengths (i.e., the anisotropy distribution function). In a sense, the observed powder spectrum $S(\omega)$ can equally well be described by either of the two expressions (*1*):

$$\begin{aligned} S(\omega) &= \int g(x)\left[p(\theta)\,\frac{\partial\theta}{\partial\omega}\right] dx, \quad \theta = \theta(x,\omega) \\ &= \int p(\theta)\left[g(x)\,\frac{\partial x}{\partial\omega}\right] d\theta, \quad x = x(\theta,\omega), \end{aligned} \qquad [1]$$

where $g(x)$ is an anisotropy distribution function, and $p(\theta)$ is an orientation distribution function. Thus, the first of the above expressions is a $g(x)$-weighted superposition of lineshape functions, one for each anisotropy $x$; a classic example of a lineshape function would be a powder pattern of a single chemical shift anisotropy in $^{31}$P NMR. The second expression is a $p(\theta)$-weighted superposition of spectra from the individual oriented domains that constitute the powder sample, one for each orientation $\theta$. For example, in a sample with a random distribution of orientations, $p(\theta) \propto \sin(\theta)$.

Macroscopically orienting the sample reduces $p(\theta)$ to a delta function and thus the observed spectrum is a direct measure of the anisotropy distribution $g(x)$. The difficulty arises when this macroscopic orientation is not perfect. Fortuitously, even a slight degree of preferred orientation along $\theta = 90^\circ$ tends to produce very narrow and well-resolved peaks which one tends to associate with oriented samples. This is a simple consequence of the fact that from

$$\omega(x,\theta) = x\,P_2(\cos\theta) = x\,\frac{3\cos^2\theta - 1}{2} \qquad [2]$$

it follows that

$$p(\theta)\frac{\partial x}{\partial\omega} = -\frac{p[\theta(x,\omega)]}{[2(x-\omega)(x+2\omega)]^{1/2}}, \qquad [3]$$

which diverges at $\omega = -x/2$, i.e., at $\theta = 90^\circ$, resulting in strong peaks even in powder samples. With a bit of baseline manipulation, one is easily fooled into seeing narrow peaks of a "perfectly" oriented domain. Unfortunately, that is often not the case.

The need to characterize $p(\theta)$ has recently become even more urgent, with the increasing use of bicelles (*2*) as the medium of choice for creating oriented samples of proteins—a step that greatly improves the chances of unambiguously determining native protein structure from NMR, X-ray, and/or neutron scattering data. In addition, even the traditional method of orienting samples by depositing them on glass or mica substrate has been known to produce significant "mosaic spread" of orientations (*3*). At the other extreme end, in the case of truly random orientational distribution $p(\theta) \propto \sin\theta$, a numerical technique



1090-7807/01 $35.00

of dePakeing (*4–7*) has been developed and used extensively to extract $g(x)$ when $p(\theta)$ was known. Because of the symmetric relationship between $g(x)$ and $p(\theta)$ implied by Eq. [1], the complementary form of dePakeing, in which $g(x)$ was known and $p(\theta)$ was extracted from the measured data, has also been developed and used to determine the orientational distribution of a liquid crystal (mixture M5) trapped in the channels of a microporous material (Anopore, $Al_2O_3$) that was mechanically rotated in the magnetic field (*8*); $g(x)$ was supplied in the form of 18 chemical shift parameters and $p(\theta)$ was calculated as a discrete function defined at 50–100 points in the range $\theta = 0$–$90°$.

More recent developments have made it possible to extract both the true $g(x)$ and a limited estimate of $p(\theta)$ *simultaneously* (*1*). This allows dePakeing even in the presence of nonrandom orientational distributions within the powder sample, such as may arise under the influence of the magnetic field on the model membrane systems with anisotropic magnetic susceptibility. In addition, however, one obtains an independent measure of $p(\theta)$ that provides information on the structural organization of the system. In particular, multilamellar vesicles have been seen to undergo a magnetically induced deformation to a shape that qualitatively could be described as an ellipsoid with its long axis along the magnetic field and the ratio of the long-to-short semi-axes of about 2–6. This was true of a broad range of phospholipids and phospholipid mixtures and was observed at fields as low as 7 T. Intense numerical requirements necessarily limited the range of possible forms of $p(\theta)$ that could be considered. In addition, at small deviations from randomness, differentiation between various analytical forms of $p(\theta)$ is poor, as they all must approach $\sin\theta$ in the limit of a nearly random distribution.

We have recently been able to adapt these methods to bicelles or bilayers oriented on glass plates, where the orientational distribution function appears to consist of two components, only one of which has a certain preferred orientation, whether magnetically (bicelles) or mechanically (glass plates) induced. In the case of 1,2-dimyristoyl-*sn*-glycero-3-phosphocholine : 1,2-dicaproyl-*sn*-glycero-3-phosphocholine (DMPC : DHPC, and their chain-deuterated analogues) bicelles, the capabilities of our numerical method can be illustrated by the following two figures. In Fig. 1, the spectrum is analyzed in terms of a single analytical form of $p(\theta)$, namely that of an ellipsoid of rotation with its long axis along the magnetic field:

$$p_{\kappa_E}(\theta) \propto \sin\theta\,[1 - (1 - \kappa_E)\cos^2\theta]^{-2}. \qquad [4]$$

This model form of $p(\theta)$ is easy to visualize as a magnetically induced deformation of a multilamellar lipid vesicle; it represents one end of the range of possible functional forms, in which adjacent domains maintain highly correlated orientations. The parameter $\kappa_E$ has a simple geometrical meaning of the square of the ratio of the long to short semi-axes. For $\kappa_E = 1$ the ellipsoid reverts to a sphere, and thus the random powder distribution is recovered, while at high $\kappa_E$ values the shape approaches a cylinder with its axis along the external magnetic field, and all surface normals are along a single direction $\theta = 90°$ to the magnetic field. This ability to cover the entire range of shapes of $p(\theta)$—from a random spherical distribution to a fully oriented one at $\theta = 90$ (for $\kappa_E \gg 1$)—in a continuous manner is an important feature of any candidate model. Several have been tested previously (*1*) and also applied to the data shown in Fig. 1; in the observed range of deviations from random distribution the quality of fit does not depend greatly on which model is used, provided that the model allows for a partially oriented phase that accounts for the reduced spectral intensity in the wings of the powder pattern. More importantly, the extracted "dePaked spectrum," or essentially $g(x)$, is very similar for all models we tested, as long as convergence (see below) is achieved. Sometimes it was not, indicating that a particular model was not suitable. We settled on the ellipsoidal description of the orientational distribution function to have an easy instinctive grasp of the meaning of the orientational model parameter $\kappa_E$, but other descriptions of the deviations from random orientational distribution are possible. A better signal-to-noise ratio is required to provide differentiation between models by selecting the lowest of all possible minima of the misfit function (*1*).

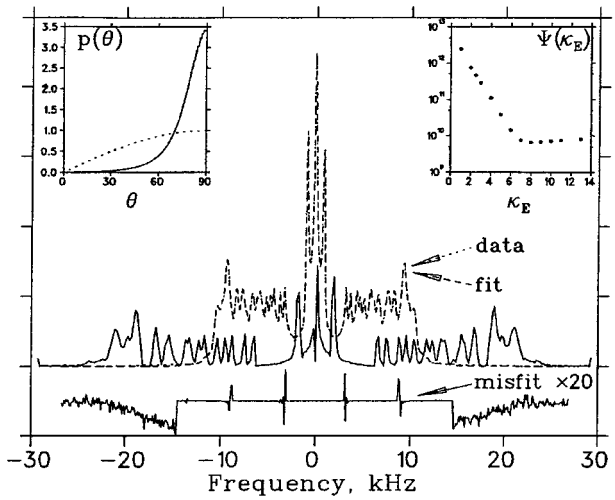


**FIG. 1.** DePakeing of a $^2$H NMR spectrum using an ellipsoidal orientational distribution model.

The convergence is reported by a minimum (with respect to $\kappa_E$) of a quadratic misfit function calculated over the entire spectrum

$$\Psi[g(x);\kappa_E] = \int [S(\omega) - \tilde{S}(\omega)]^2 + \lambda\,|g''|^2 \qquad [5]$$

subject to $g(x) \geq 0$. Here $\tilde{S}(\omega)$ is calculated using Eq. [1], where $p(\theta)$ has been substituted from Eq. [4] for a given value of $\kappa_E$. The symbol $\lambda$ is the regularization parameter determined by a self-consistent method of Honerkamp and Weese (*10*) and $g''$ denotes the second derivative of the distribution function $g(x)$.

The minimum yields a reasonable approximation of $g(x)$, consistent with the input data $S(\omega)$. This is, in essence, the Tikhonov regularization method (*11*) of inverting the Fredholm integral equation of the second kind (Eq. [1]) to obtain $g(x)$ from a measured $S(\omega)$. Note how good the fit is: the input data (dotted line) and the fit (dashed line) coincide on the plot; only by looking at a greatly enlarged *difference* between the two (marked "misfit" in Fig. 1 and shown $\times 20$ on the vertical scale) can one see small systematic differences in the wings of the spectrum. Despite that, this fit was *rejected!*

The small systematic differences between the input data and the fit are actually very significant. The human eye is not very good at distinguishing slight lineshape differences between "data" and "model"; thus the traditional way of judging visually the quality of the fit is not only very approximate, but could be also misleading. Only when acquired spectra are of high fidelity *and* when precise numerical work with a sufficient number of degrees of freedom is performed, may the minute systematic differences between the data and the model be interpreted and, in fact, reveal the deficiency of the model and a need for a better one. For example, by converting the spectral information into the distribution of anisotropies, $g(x)$, and monitoring the misfit, we were able to fine-tune the phasing of our spectra to within $0.1^\circ$, a nontrivial exercise when performed by the eye directly on the spectrum, $S(\omega)$.

The conversion from $S(\omega)$ to $g(x)$ is not a unitary, reversible transformation. The essence of our numerical strategy is that the fit proceeds until the statistics of the misfit is exactly equal to the statistics of the noise distribution in the baseline of the spectrum. Zero misfit in the central part of Figs. 1–3 is a consequence of having a sufficiently high signal-to-noise ratio in the data and the use of a high grid density necessary to account for the sharp features of the spectrum made up of multiple Pake doublets. Lowering this grid density leads to a significant increase in the misfit. As a side effect of this high grid density, noise is treated as systematic intensity as well in the regions of high signal-to-noise ratio. Thus, experimental noise does appear in $g(x)$. The resulting $g(x)$ should not be considered a "model function" produced by a fit but rather a model-free remapping of input data into a different representation, namely that of a distribution of anisotropies.

Consider the misfit shown in Fig. 2 at $\times 50$ vertical scale. There is no systematic difference between the input data (the spectrum) and the fit curve, and the minimum of the quadratic misfit function $\Psi$ is now significantly deeper than in Fig. 1 (note the log scale of the right-hand inserts). In order to achieve such quality of fit, we needed to accommodate the shoulder intensity by including into our model $p(\theta)$ *two* separate terms: an elliptical distribution of Eq. [4] as well as a spherically symmetric term $\propto \sin\theta$. The relative contribution of the two components was the second fit parameter, and the global minimum shown corresponds to $25 \pm 2\%$ spherical, $75 \pm 2\%$ ellipsoidal distribution, as well as $\kappa_E = 15 \pm 0.5$ for the elliptical part. Note the subtle changes in the form of $p(\theta)$ in the insert on the left, compared

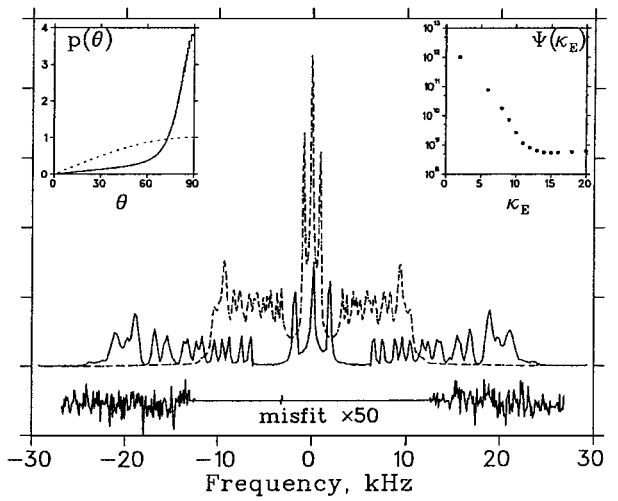


**FIG. 2.** DePakeing of a $^2$H NMR spectrum using a mixed orientational distribution model.

to that of Fig. 1. Independent of the particulars of the model used to parametrize $p(\theta)$, the low-intensity shoulder extending to low $\theta$ values is essential, as it reflects the actual distribution of the orientations that individual domains have in our sample. Extraction of the true order parameter (anisotropy) distribution $g(x)$ as represented by the dePaked spectrum (the solid line in Fig. 2) is the main goal of the procedure, as it reports on the nature of the molecular motions, but the parameters extracted as part of $p(\theta)$ model distribution are helpful in establishing gross organizational structure in the sample. In this particular case of a perdeuterated lipid sample in a $q = 4.4$ DMPC : DHPC mixture, a detailed analysis of the spectrum led us to a partial phase diagram of what turned out to be a rather complicated multicomponent system (*9*), with various structural phases exhibiting greatly varying degrees of preferential orientation, a result of considerable importance for the use of bicelles as an orienting medium for protein structure determination.

Even in cases where a "well-defined" orientational distribution has traditionally been assumed, such as in mechanically oriented model membrane systems on glass substrates, the use of our numerical methods can yield revealing results. For example, lipid bilayers can preferentially orient along the substrate surface by drying vesicle suspensions or by pelleting them in the centrifuge on an isopotential surface. Simultaneous drying with centrifugation has been shown to increase the degree of orientation, both for lipid only and for lipid-protein reconstituted membranes (*12*). We adapted this isopotential spin-dry centrifugation approach and prepared a sample of oriented 1-stearoyl-$d_{35}$-2-*sn*-oleoyl-*sn*-glycero-3-phosphocholine ($d_{35}$-SOPC) by drying liposome suspension on a 12-mm round glass slide placed in a custom-made insert for SW-28 swinging-bucket rotors of a Beckman centrifuge spinning at 18,000 rpm. The glass "sandwich" was then assembled, hydrated in excess water, and equilibrated at about 25°C for several hours. We used 0.5–1.5 mg of

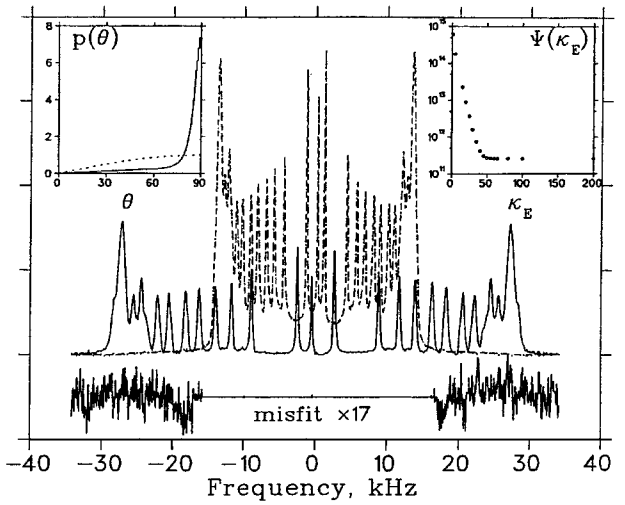


**FIG. 3.** Glass-slide oriented sample has a significant unoriented component.

lipid per slide and 1–2 slides per sample. The spectrum, measured when the normal to the bilayer is at 90° to the external magnetic field, is processed in a manner described above, as shown in Fig. 3. The observed $^2$H NMR spectrum appears to be highly oriented. Only upon a close examination can one see the remnants of the shoulders of the Pake pattern. We use the same mixed-model approach to establish that the best convergence is achieved when the spectrum is assumed to consist of a highly oriented fraction ($74 \pm 1\%$ of the sample) and a fraction that is close to a randomly oriented powder ($26 \pm 1\%$). Significantly, interpretation of the highly oriented fraction in terms of an ellipsoidal orientational distribution fails to converge at a specific $\kappa_E$ value: all values $\kappa_E \geq 60$ represent equally good fits to the data, within the constraints of a given signal-to-noise ratio. This is an indication that this particular geometric interpretation may not be appropriate for this spectrum, and that a different model may need to be devised. Nevertheless, the calculation yields an important lower bound: had the ellipsoidal model been appropriate, the value of $\kappa_E$ most compatible with the data would have been at least 60, i.e., the ratio of the semi-axes of at least 7.8. This characterizes qualitatively the width of the orientational distribution function, i.e., the so-called mosaic spread of the domains oriented by the glass plates. The misfit (shown below the two coinciding lines of the data and fit) is again minimal, and the systematic misfit is of the same order of magnitude as the random noise in the spectrum. Thus, even when the algorithm fails to converge to a unique value, a meaningful interpretation can be made.

We repeated the above analysis using other models developed earlier (*1*), and the results are not substantially different. For example, using the Boltzmann model,

$$p_E(\theta) \propto \sin\theta \exp[\kappa_E \cos^2\theta], \qquad [6]$$

yields a result essentially identical to that of Fig. 3, with a flat tail in $\Psi(\kappa_E)$ extending to large negative values of $\kappa_E$. Understandably for the given signal-to-noise ratio, any model that allows the existence of a narrow peak in $p(\theta)$ near $\theta = 90°$ is adequate. A better model and a better signal-to-noise ratio are needed to refine the above qualitative result. It must be pointed out, however, that the determination of the distribution of anisotropies $g(x)$ ($^2$H NMR order parameters in this case, the solid lines in Figs. 2 and 3) is robust and does not depend on knowing the exact details of $p(\theta)$.

In conclusion, we have demonstrated how a precise numerical analysis of all available spectroscopic information can yield important insights into the nature of structurally complex multicomponent systems, such as DMPC : DHPC bicelles or oriented systems supported by glass plates. However, the lessons learned—the need for high-fidelity NMR spectra, appropriately flexible parametrization choice, precise regularization of the fit to achieve stability, careful attention to the nature of the misfit—all apply within a much more general context of measuring and interpreting one's spectroscopic data.

## ACKNOWLEDGMENTS

Our calculations have been greatly assisted by access to Biowulf, a cluster of computers developed at the NIH. The figures were prepared using the software developed at TRIUMF (Vancouver, British Columbia). ES acknowledges the financial support of the Natural Sciences and Engineering Research Council of Canada and the intramural support from the Laboratory of Membrane Biochemistry and Biophysics, NIAAA, NIH, during the sabbatical stay.

## REFERENCES

1. H. Schäfer, B. Mädler, and E. Sternin, *Biophys. J.* **74,** 1007 (1998).
2. C. Sanders and J. Schwonek, *Biochemistry* **31,** 8898 (1992).
3. K. Arnold, K. Gawrisch, and F. Volke, *Stud. Biophys.* **75,** 189 (1979).
4. M. Boom, J. H.Davis, and A. L. Mackay, *Chem. Phys. Lett.* **80,** 198 (1981).
5. E. Sternin, M Bloom, and A. L. Mackay, *J. Magn. Reson.* **55,** 274 (1983).
6. H. Schäfer, B. Mädler, and F. Volke, *J. Magn. Reson. A* **116,** 145 (1995).
7. M. A. McCabe and S. R. Wassal, *Solid State Nucl. Reson.* **10,** 53, (1997).
8. H. Schäfer and R. Stannarius, *J. Magn. Reson. B* **106,** 14 (1995).
9. E. Sternin, D. Nizza, and K. Gawrisch, Submitted for publication (2000).
10. J. Honerkamp and J. Weese, *Contin. Mech. Thermodyn.* **2,** 17 (1990).
11. A. N. Tikhonov V. Y. Arsenin, "Solutions of Ill-Posed Problems," Wiley, New York (1977).
12. G. Groebner, A. Taylor, P. Williamson, G. Choi, C. Glaubits, J. Watts, W. de Grip, and A. Watts, *Anal. Biochem.* **254,** 132 (1997).